Electronic Supplementary Material (ESI) for CrystEngComm.

Supplementary Information

Disclosing the Electronic Structure and Optical Properties of $Ag_4V_2O_7$ crystals: Experimental and Theoretical Insights

R.C. de Oliveira[a], L. Gracia[b], M. Assis[a], M. Siu Li[c], J. Andres[b], E. Longo[d], L.S. Cavalcante[e]*

[a]*INCTMN-UFSCar, Universidade Federal de São Carlos, P.O. Box 676, 13565–905, São Carlos, SP, Brazil.*

[b]*Departament de Química Física i Analítica, Universitat Jaume I, 12071, Castelló de la Plana, Spain.*

[c]*IFSC-Universidade de São Paulo, P.O. Box 369, 13560-970 São Carlos, São Paulo, Brazil*

[d]*INCTMN-UNESP, Universidade Estadual Paulista, P.O. Box 355, 14801–907 Araraquara, SP, Brazil*

[e]*PPGQ-Universidade Estadual do Piauí, Rua João Cabral, 2231, P.O. Box 381, 64002–150, Teresina, PI, Brazil.*

**laeciosc@gmail.com*;

Experimental details

The precursors utilized in this synthesis were silver nitrate, $AgNO_3$ (99,0% purity, Synth) and ammonium monovanadate, NH_4VO_3 (99% purity, Aldrich). Initially, 1×10^{-3} mol de NH_4VO_3 were dissolved in 60 mL distilled water at 30°C, under magnetic stirring for 15 minutes. Then, 1×10^{-3} mol of $AgNO_3$ were dissolved in 15 mL distilled water, under magnetic stirring for 15 minutes, to this solution was added a few drops of ammonium hydroxide (NH_4OH) (30% in NH_3, Synth) until the solution becomes clear. Both solutions were quickly mixed, promoting the instantaneous formation of solid $Ag_4V_2O_7$ precipitates (orange coloration). To accompany the change of morphologies, the PM was performed at 30 ºC for 10 min. The precipitate was centrifuged, washed with distilled water several times, and dried in a conventional furnace at 60 ºC for some hours.

Characterization

X-ray diffraction using a Rigaku-DMax/2500PC (Japan) with Cu Kα radiation (λ = 1.5406 Å) in the 2θ range from 10° to 80° with a scanning rate of 0.02°/min. Micro-Raman spectroscopy was carried out using an T64000 spectrometer (Horiba obin-Yvon, Japan) coupled to a CCD Synapse detector and an argon-ion laser, operating at 514 nm with maximum power of 7 mW. The spectra were measured in the range from 100 cm^{-1} to 1100 cm^{-1}. UV-vis spectra were obtained in a Varian spectrophotometer model Cary 5G (USA) in diffuse reflection mode. The morphologies were investigated with a field emission scanning electron microscopy (FE-SEM) Supra 35-VP Carl Zeiss (Germany) operated in 15 KV. The PL measurements were performed with a Monospec 27 monochromator Thermal Jarrel Ash (USA) coupled to a R446 photomultiplier Hamamatsu Photonics (Japan). A krypton ion laser Coherent Innova 90 K (USA) (λ = 350 nm) was used as excitation source, keeping its maximum output power at 500 mW. All experiments measurements were performed at room temperature.

Theoretical Calculations

Calculations on the periodic $Ag_4V_2O_7$ structure were performed with the CRYSTAL14 sofware package /Dovesi R.; Saunders, V. R.; Roetti, C.; Orlando, R.; Zicovich-Wilson, C. M.; Pascale, F.; Civalleri, B.; Doll, K.; Harrison, N. M.; Bush, I. J.; D'Arco, P.; Llunell, M.; Causà M.; Noël Y., *Crystal14 User's Manual*. University of Torino: Torino, 2014./ Tungsten was described by a large-core ECP, derived by Hay and Wadt, and modified by Cora *et al*. /Cora, F.; Patel, A.; Harrison, N. M.; Dovesi, R.; Catlow, C. R. A. An Ab Initio Hartree-Fock Study of the Cubic and Tetragonal Phases of Bulk Tungsten Trioxide. *J. Am. Chem. Soc.* **1996**, *118*, 12174-12182./ Silver and oxygen centers were described using HAYWSC-311d31G and O (6-31d1G) basis sets, respectively, which were taken from the Crystal web site./

http://www.crystal.unito.it/Basis_Sets/Ptable.html/ A Range-separated hybrid functional, the screened-Coulomb HSE06 was used in order to give the accurate band gaps for the computed structures. The diagonalization of the Fock matrix was performed at adequate *k*-points grids in the reciprocal space. The thresholds controlling the accuracy of the calculation of the Coulomb and exchange integrals were set to10^{-8} and 10^{-14}, and the percent of Fock/Kohn-Sham matrices mixing was set to 40 (IPMIX keyword)./Dovesi R.; Saunders, V. R.; Roetti, C.; Orlando, R.; Zicovich-Wilson, C. M.; Pascale, F.; Civalleri, B.; Doll, K.; Harrison, N. M.; Bush, I. J.; D'Arco, P.; Llunell, M.; Causà M.; Noël Y., *Crystal14 User's Manual*. University of Torino: Torino, 2014./ The empirical correction scheme to energy that considers the long-range dispersion contributions proposed by Grimme/ S. Grimme, *Journal of Computational Chemistry* 2006, *27*, 1787-1799/ and implemented by Bucko et al./ T. Bucko, J. Hafner, S. Lebegue, J. G. Angyan, *Journal of Physical Chemistry A* 2010, *114*, 11814-11824/ for periodic systems was used. In the relaxed configuration, the forces on the atoms are less than 0.0001 hartree/bohr = 0.005 eV/Å, and deviations of the stress tensor from a diagonal hydrostatic form are less than 0.1 GPa. The band structure and the density of states (DOS) projected on atoms and orbitals of bulk $Ag_4V_2O_7$ was constructed along the appropriate high-symmetry directions of the corresponding irreducible Brillouin zone. The vibrational-frequencies calculation in CRYSTAL is performed at the Γ-point within the harmonic approximation, and the dynamic matrix is computed by the numerical evaluation of the first derivative of analytical atomic gradients.

a)

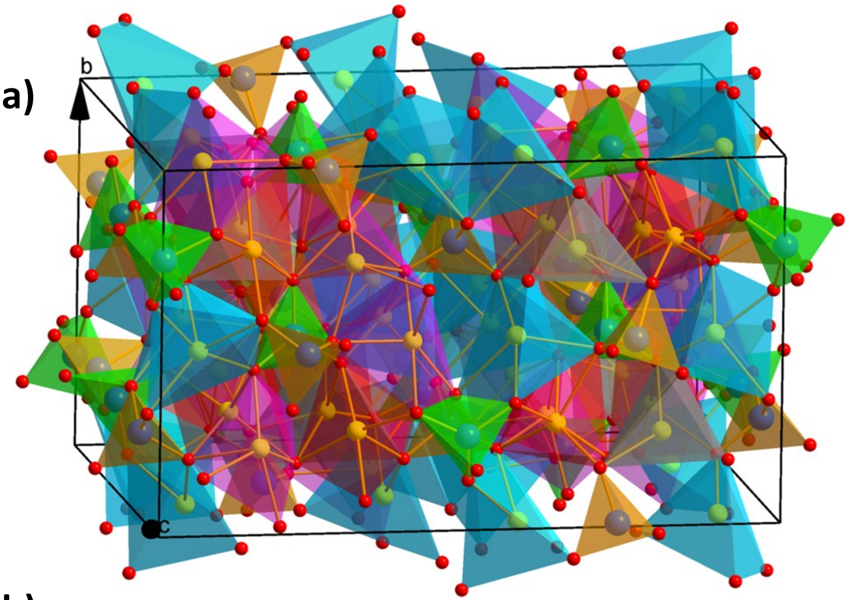

Atom	Lig	Dmin	Dmax
Ag1	5	2.271	2.636
Ag2	6	2.31	2.906
Ag3	6	2.317	2.657
Ag4	6	2.366	2.96
Ag5	6	2.438	2.982
Ag6	6	2.332	2.811
Ag7	5	2.255	2.672
Ag8	5	2.336	2.494
V1	5	1.708	2.158
V2	4	1.708	1.769
V3	4	1.707	1.788
V4	5	1.698	2.258

b)

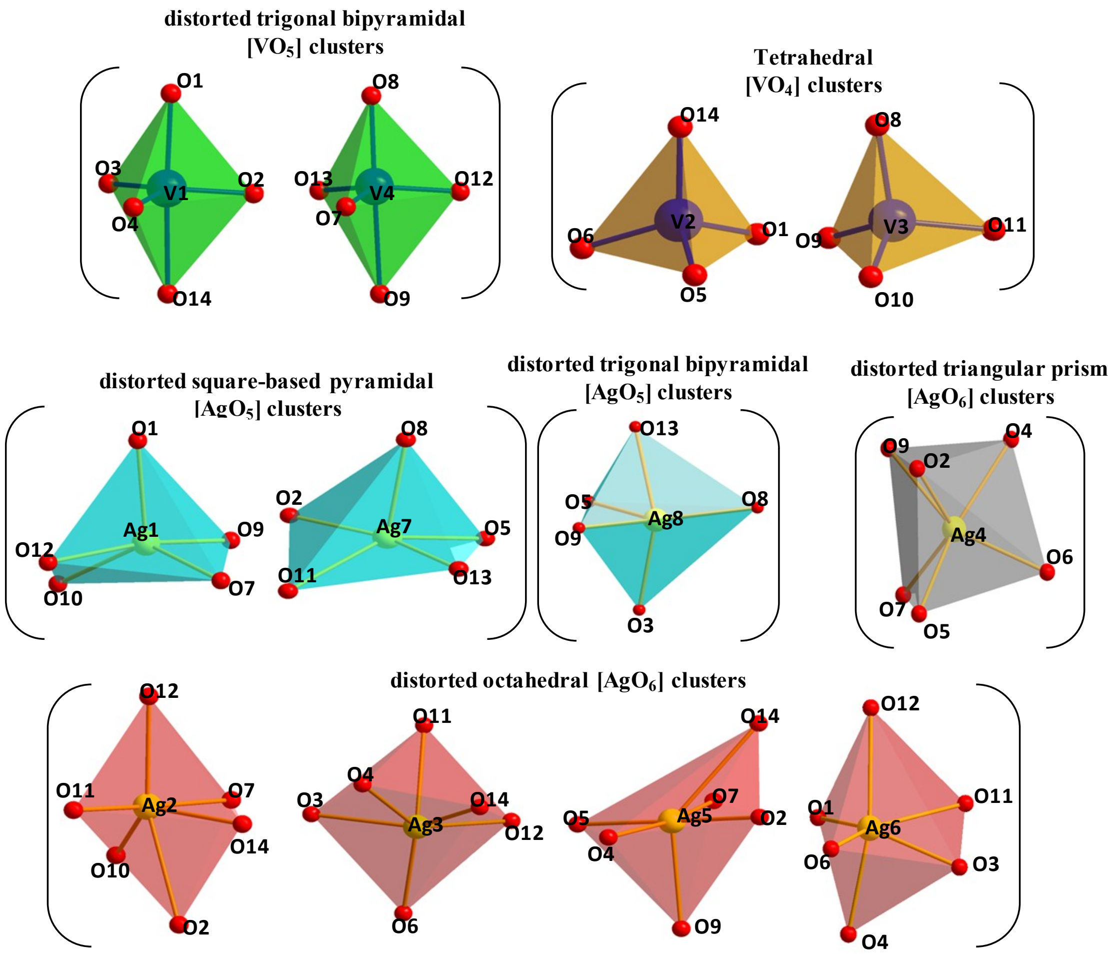

Fig. S1: **(a)** show a schematic representation of orthorhombic $Ag_4V_2O_7$ unit cell in which the different clusters, i.e. the local coordination of V and Ag atoms are depicted. **(b)** molecular geometry, and coordination of each cluster in $Ag_4V_2O_7$ crystals.

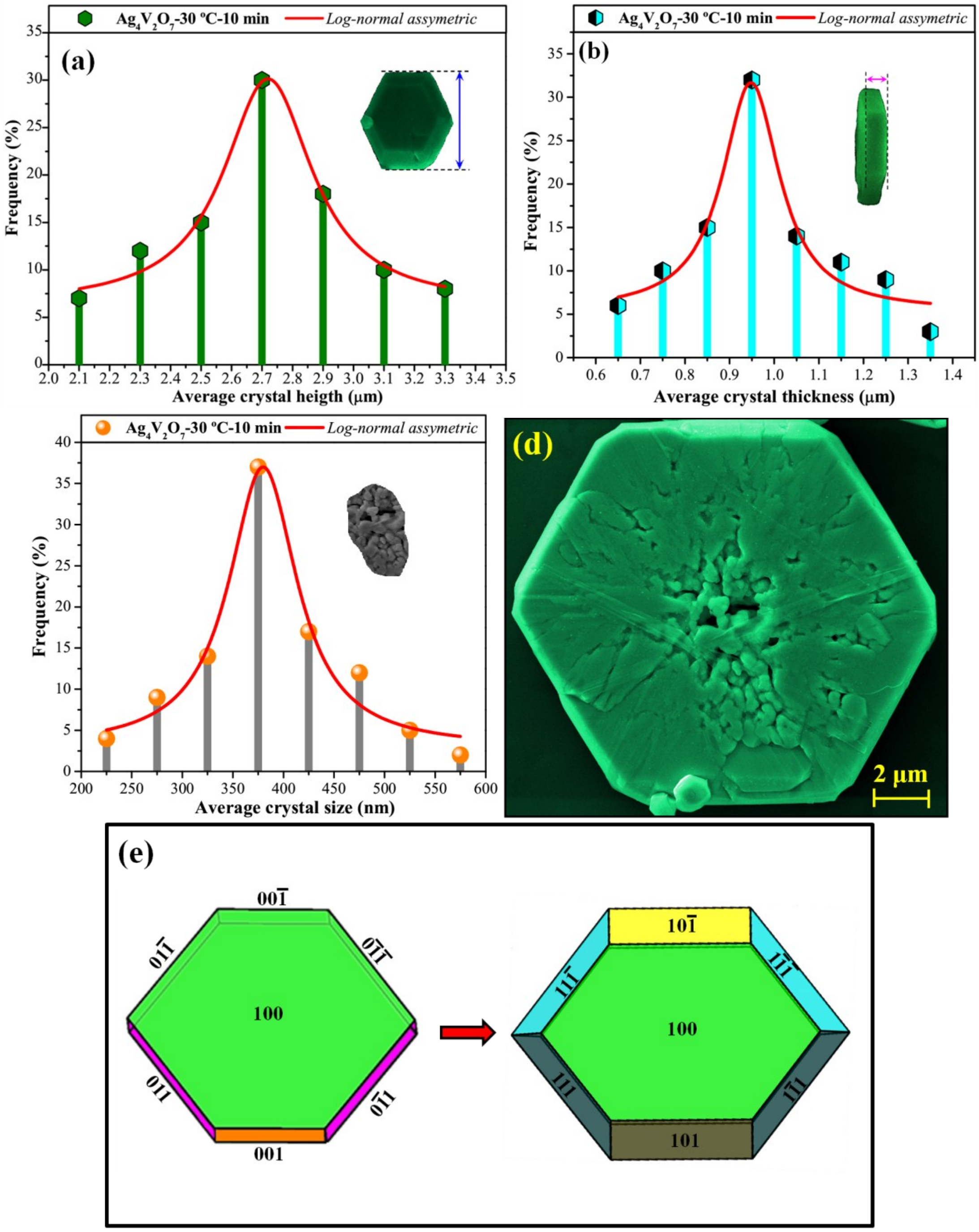

Figs. S2: **(a)** Average crystal height distribution and (b) Average crystal thickness distribution, **(c)** Average crystal size distribution of small presents into the $Ag_4V_2O_7$ microcrystals **(d)** FE-SEM images of an individual $Ag_4V_2O_7$ microcrystals and **(e)** Crystal shape simulated computationally for 3D hexagons-like $Ag_4V_2O_7$ microcrystals with 8 faces and 14 faces, respectively.

Table 1: **(a)** Lattice parameters, unit cell volume, atomic coordinates, and site occupation obtained by rietveld refinement data for the 3D hexagons-like $Ag_4V_2O_7$ microcrystals obtained at 30 ºC for 10 min and (b) Data obtained from DFT calculations for $Ag_4V_2O_7$ microcrystals

(a) $Ag_4V_2O_7$ (Rietveld refinement)				
Atoms	Wyckoff	*x*	*y*	*z*
Ag1	8c	0.91648	0.00724	0.88767
Ag2	8c	0.91424	0.00080	0.12302
Ag3	8c	0.17269	0.22475	0.90064
Ag4	8c	0.17000	0.75148	0.12172
Ag5	8c	0.83569	0.24967	0.62928
Ag6	8c	0.33870	0.74855	0.65735
Ag7	8c	0.08971	0.49878	0.14015
Ag8	8c	0.08720	0.50628	0.87029
V1	8c	0.25970	0.98828	0.75072
V2	8c	0.25995	-0.01414	0.01694
V3	8c	-0.00048	0.75612	0.72982
V4	8c	0.49883	0.25563	0.49753
O1	8c	0.21073	0.47325	0.62457
O2	8c	0.32996	0.41715	0.74135
O3	8c	0.17766	0.09133	0.30430
O4	8c	0.25982	0.35742	0.26332
O5	8c	0.16672	0.56642	0.00812
O6	8c	0.29759	0.84466	0.02677
O7	8c	0.43561	0.33066	-0.00217
O8	8c	0.02548	0.18388	0.39472
O9	8c	0.06760	0.81591	0.22975
O10	8c	-0.01673	0.85708	0.81366
O11	8c	0.42149	0.66246	0.76791
O12	8c	0.41501	0.83280	0.51010
O13	8c	0.00632	0.36942	0.08602

O14	8c	0.28365	0.99945	0.41432

a = 18.7993(9) Å, *b* = 10.85376(3) Å, *c* = 13.9028(4) Å, α = β = γ = 90°,
V = 2836.77(18) Å^3, R_{Bragg} = 3.56%, R_{wp} = 7.74%, R_p (%) = 5.62%, χ^2 = 1.427 and *S* = 1.1945

(b) $Ag_4V_2O_7$ (DFT calculations)

Atoms	Wyckoff	x	y	z
Ag1	8c	-0.0857	-0.0006	-0.1104
Ag2	8c	-0.0787	0.0127	0.1284
Ag3	8c	0.1757	0.2079	-0.1103
Ag4	8c	0.1796	-0.2323	0.1006
Ag5	8c	-0.1634	0.2395	-0.3506
Ag6	8c	0.3427	-0.2514	-0.3499
Ag7	8c	0.0933	-0.4904	0.1186
Ag8	8c	0.0773	0.4713	-0.1333
V1	8c	0.2508	-0.0272	-0.2612
V2	8c	0.2629	-0.0125	-0.0077
V3	8c	0.0007	-0.2719	-0.2651
V4	8c	0.4965	0.2472	0.4873
O1	8c	0.2183	0.4619	-0.4
O2	8c	0.3279	0.392	-0.2813
O3	8c	0.1784	0.1043	0.2871
O4	8c	0.2539	0.3731	0.2397
O5	8c	0.1649	-0.4214	-0.0264
O6	8c	0.2895	-0.1587	0.0126
O7	8c	0.4130	0.321	-0.01
O8	8c	-0.0054	0.1934	0.3806
O9	8c	0.0716	-0.1316	0.2374
O10	8c	0.0025	-0.1718	-0.168
O11	8c	0.4218	-0.3497	-0.2349
O12	8c	0.4293	-0.157	0.499
O13	8c	0.0063	0.3818	0.071
O14	8c	0.2897	0.0075	0.3875

a = 18.752 Å, *b* = 11.090 Å, *c* = 13.504 Å, α = β = γ = 90°, V = 2808.29 Å^3

Table S2: Calculated Raman-active modes from optimized orthorhombic structure of $Ag_4V_2O_7$ crystals.

mode	ω (cm^{-1})	mode	ω (cm^{-1})	mode	ω (cm^{-1})	mode	ω (cm^{-1})	mode	ω (cm^{-1})	mode	ω (cm^{-1})	mode	ω (cm^{-1})	mode	ω (cm^{-1})
Ag	13.91	Ag	65.13	B1g	93.51	B3g	162.30	B1g	243.09	B2g	351.35	Ag	440.05	B3g	800.86
B1g	27.48	B3g	66.58	Ag	94.33	B2g	163.15	Ag	244.58	Ag	351.85	B3g	444.25	B1g	803.52
B2g	31.25	B2g	67.04	B3g	94.36	B2g	165.83	B2g	245.56	B1g	357.74	B2g	448.70	Ag	807.52
B1g	35.55	Ag	67.30	Ag	96.19	Ag	165.99	B1g	251.69	Ag	358.96	B3g	449.04	B2g	809.54
B2g	36.73	B1g	67.50	B2g	97.44	B1g	168.27	B2g	261.91	B1g	360.05	B1g	452.14	B2g	810.08
Ag	37.75	B2g	67.74	B3g	98.73	B2g	172.09	B3g	263.12	B3g	361.69	Ag	454.01	B3g	819.43
B3g	38.46	B2g	69.31	B2g	100.03	B1g	173.29	Ag	263.35	B2g	365.35	B2g	455.92	B1g	819.78
Ag	39.25	B1g	69.40	B1g	100.59	Ag	174.56	B3g	272.86	B1g	367.51	B3g	459.63	Ag	819.90
B1g	40.92	B3g	69.68	B3g	104.06	B3g	175.17	B1g	274.15	Ag	368.16	B3g	468.11	B1g	827.30
B3g	42.43	B1g	70.81	B1g	106.94	B3g	175.64	B2g	274.22	B3g	368.43	B1g	471.55	B2g	827.99
Ag	42.78	Ag	72.34	Ag	107.86	B1g	176.92	Ag	275.88	B2g	370.82	B2g	473.45	Ag	829.05
B3g	44.09	B2g	72.45	B2g	107.88	B1g	181.91	B3g	279.99	B3g	372.51	Ag	473.56	B3g	833.82
Ag	44.80	B3g	72.50	B3g	107.90	B2g	184.57	B1g	282.51	Ag	377.91	B2g	490.26	Ag	838.04
B3g	46.44	B1g	73.38	B3g	110.86	B3g	188.11	B2g	284.62	B1g	380.49	B1g	490.44	B2g	839.60
Ag	47.03	Ag	74.16	Ag	111.41	B1g	188.19	B1g	290.14	B3g	381.60	B3g	505.31	B3g	840.88
B2g	47.39	Ag	74.54	Ag	115.31	B2g	189.27	B2g	291.91	B2g	382.61	Ag	508.40	B1g	840.99
B2g	48.20	B2g	74.55	B2g	117.54	Ag	192.36	Ag	292.03	B1g	386.09	B3g	681.44	Ag	841.18
B1g	48.90	B3g	75.32	B1g	118.04	B3g	195.48	B1g	294.60	B2g	388.30	Ag	682.16	B1g	843.56
Ag	49.07	B1g	75.34	B1g	120.32	B1g	197.94	B3g	302.11	Ag	390.40	B1g	687.12	Ag	845.05
B2g	49.68	B3g	76.04	Ag	124.61	B2g	199.70	B1g	303.61	B3g	396.18	B3g	691.67	B1g	849.14
B3g	51.21	Ag	77.95	B1g	126.73	Ag	200.08	Ag	306.35	Ag	397.55	B2g	695.48	B2g	849.70
B2g	51.73	B1g	78.07	Ag	132.41	B2g	202.59	B2g	306.70	B2g	405.60	B2g	702.04	B3g	853.07
B3g	52.44	B3g	80.53	B2g	132.91	B3g	205.33	B1g	311.38	B3g	406.33	Ag	702.40	B1g	858.31
B1g	52.93	B1g	80.72	B1g	133.60	Ag	207.82	B3g	312.28	B1g	407.78	B1g	704.50	B2g	862.14
Ag	53.07	B2g	81.26	B3g	136.42	B1g	208.14	Ag	312.29	B2g	412.49	B1g	741.73	B1g	864.98
B3g	53.10	B3g	81.79	Ag	137.81	B3g	208.47	Ag	315.57	B1g	414.20	Ag	744.08	B3g	870.87
B2g	55.05	B3g	83.31	B2g	139.26	B3g	208.85	B3g	316.75	Ag	414.74	B3g	746.91	Ag	875.06
B1g	55.14	B2g	83.86	Ag	140.28	Ag	210.32	B2g	318.00	B3g	417.71	B2g	750.96	B2g	875.23
Ag	55.42	B3g	84.64	B2g	141.91	B2g	210.51	B1g	320.54	B2g	418.26	Ag	754.10	B3g	883.18
B1g	56.98	Ag	84.85	B3g	141.96	B3g	211.31	B3g	328.08	Ag	421.86	B1g	757.60	B3g	890.24
B2g	59.30	B2g	85.22	B1g	144.77	Ag	217.28	B2g	330.10	B1g	423.49	B2g	759.51	B2g	901.55
B1g	59.32	B2g	86.02	Ag	145.09	B3g	218.64	B1g	330.68	B2g	425.24	B2g	773.07	B1g	902.54
Ag	59.45	B1g	86.14	B2g	148.33	B1g	219.36	Ag	333.69	Ag	426.74	Ag	776.84		
B3g	59.97	Ag	87.05	B1g	148.42	B2g	219.54	B3g	337.56	B1g	428.54	B3g	780.76		
B1g	61.18	B1g	87.16	Ag	150.36	B2g	224.10	Ag	340.02	B3g	431.29	B3g	781.62		
Ag	61.90	B3g	88.93	B3g	152.64	Ag	227.78	B2g	342.39	B2g	431.72	Ag	786.94		
B3g	62.78	B1g	89.15	Ag	152.76	B3g	232.02	B3g	343.70	B1g	433.35	B1g	791.15		
B2g	63.17	B2g	89.36	B2g	154.40	B3g	233.28	Ag	346.31	Ag	434.89	B3g	792.56		
B3g	64.14	Ag	89.89	B1g	155.54	B1g	234.76	B1g	347.65	B2g	436.40	B2g	796.09		
B1g	64.69	B2g	91.74	B3g	157.96	B2g	234.90	B3g	350.58	B1g	438.52	Ag	796.39		

Table S3: Positions of active Raman-modes (experimental and theoretical).

Types of Raman-active modes	Specific positions of the experimental Raman-active modes from Raman spectrum (cm^{-1})	Calculated theoretically positions of the Raman-active modes from optimized structure (cm^{-1})
B_{3g}		66.57
B_{2g}		67.04
A_g		67.30
B_{1g}	67	67.50
B_{2g}		67.74
B_{3g}		83.30
B_{2g}		83.86
B_{3g}		84.64
A_g	84	84.85
B_{2g}		85.22
B_{3g}		98.73
B_{2g}	100	100.03
B_{1g}		100.59
B_{2g}		165.83
A_g	166	165.99
B_{1g}		168.27
B_{1g}		243.09
A_g	243	244.58
B_{2g}		245.56
B_{2g}		261.91
B_{3g}	263	263.12
A_g		263.35
A_g	335	333.69
B_{3g}		337.56
B_{3g}	363	361.69
B_{2g}		365.35
A_g	529	508.40
B_{3g}		681.44
A_g	654	682.16
B_{1g}	672	687.12
B_{2g}	770	773.07
B_{1g}	790	791.15
B_{3g}		792.56
B_{2g}	810	809.54, 810.08
B_{1g}		827.30
B_{2g}	830	827.99
A_g		829.05
B_{3g}		833.82
B_{1g}		902.54

S4.

The structural defects associated to the electronic charge transfer processes from ordered (o) to disordered (d) clusters can be explained by the following equations (1–12):

$$[VO_4]_o^x + [VO_4]_d^x \rightarrow [VO_4]_o^{'} + [VO_4]_d^{\bullet} \quad (1)$$

$$[VO_5]_o^x + [VO_5]_d^x \rightarrow [VO_5]_o^{'} + [VO_5]_d^{\bullet} \quad (2)$$

$$[AgO_5]_o^x + [AgO_5]_d^x \rightarrow [AgO_5]_o^{'} + [AgO_5]_d^{\bullet} \quad (3)$$

$$[AgO_6]_o^x + [AgO_6]_d^x \rightarrow [AgO_6]_o^{'} + [AgO_6]_d^{\bullet} \quad (4)$$

$$[VO_4]_o^x + [VO_3.V_O^x]_d \rightarrow [VO_4]_o^{'} + [VO_3.V_O^{\bullet}]_d \quad (5)$$

$$[VO_4]_o^x + [VO_3.V_O^{\bullet}]_d \rightarrow [VO_4]_o^{'} + [VO_3.V_O^{\bullet\bullet}]_d \quad (6)$$

$$[VO_5]_o^x + [VO_4.V_O^x]_d \rightarrow [VO_5]_o^{'} + [VO_4.V_O^{\bullet}]_d \quad (7)$$

$$[VO_5]_o^x + [VO_4.V_O^{\bullet}]_d \rightarrow [VO_5]_o^{'} + [VO_4.V_O^{\bullet\bullet}]_d \quad (8)$$

$$[AgO_5]_o^x + [AgO_4.V_O^x]_d \rightarrow [AgO_5]_o^{'} + [AgO_4.V_O^{\bullet}]_d \quad (9)$$

$$[AgO_5]_o^x + [AgO_4.V_O^{\bullet}]_d \rightarrow [AgO_5]_o^{'} + [AgO_4.V_O^{\bullet\bullet}]_d \quad (10)$$

$$[AgO_6]_o^x + [AgO_5.V_O^x]_d \rightarrow [AgO_6]_o^{'} + [AgO_5.V_O^{\bullet}]_d \quad (11)$$

$$[AgO_6]_o^x + [AgO_5.V_O^{\bullet}]_d \rightarrow [AgO_6]_o^{'} + [AgO_5.V_O^{\bullet\bullet}]_d \quad (12)$$

where, $[VO_4]_d^x$, $[VO_5]_d^x$, $[AgO_6]_d^x$, $[AgO_5]_d^x$, $[VO_4.V_O^x]_d$, $[VO_5.V_O^x]_d$, $[AgO_5.V_O^x]_d$, and $[AgO_6.V_O^x]_d$ are electron donors; $[VO_4.V_O^{\bullet}]_d$, $[VO_5.V_O^{\bullet}]_d$, $[AgO_5.V_O^{\bullet}]_d$, and $[AgO_6.V_O^{\bullet}]_d$ are electron donors/acceptors; and $[VO_4]_o^x$, $[VO_5]_o^x$, $[AgO_5]_o^x$, and $[AgO_6]_o^x$ are electron acceptors.

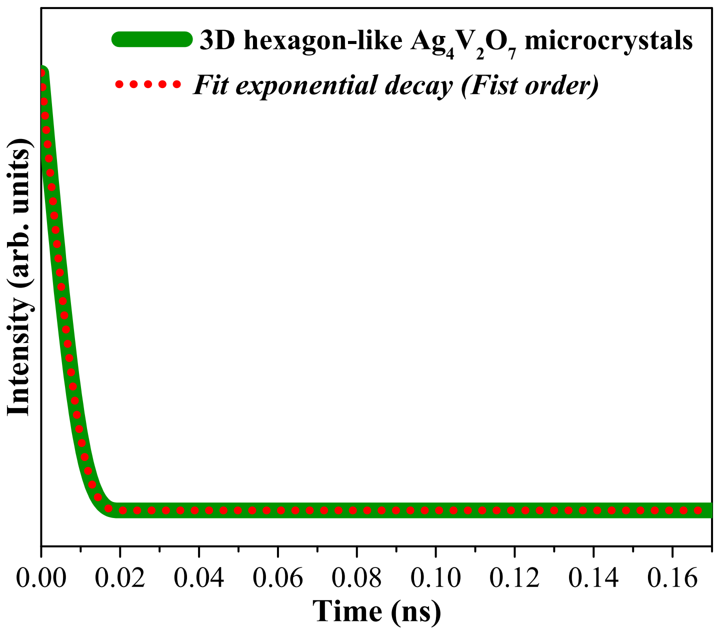

Figs. S3: Luminescence decay of 3D hexagon-like $Ag_4V_2O_7$ microcrystals [excitation wavelength (λ_{exc} = 350 nm)] monitoring the maximum PL emissions at (450 nm).